Progress In Electromagnetics Research C, Vol. 124, 243–252, 2022

New Dual-Passband SIW Filter with Loaded T-Slot

Mingming Gao, Min Li*, Jingchang Nan, and Yuan Wang

Abstract—In order to effectively improve filter selectivity and out-of-band rejection level, a multi-cavity two-mode dual-passband filter operating in X-band is proposed. By designing a suitable circuit topology, the bandpasss of the filter are formed using TE_{201} mode in the substrate integrated waveguide (SIW) cavity and the TE_{101} mode in the half mode substrate integrated waveguide (HMSIW) cavity. In addition, incorporating a T-slot structure in the dual-mode SIW cavity can add additional transmission zeros (TZs) and improve the filter selectivity while achieving miniaturization. The center frequencies of the two passbands are 8.67 GHz and 11.52 GHz, respectively. The inter-band isolation is better than 65 dB with three transmission zeros and maximum insertion loss of 0.48 dB and 0.31 dB, respectively. The proposed filter has a compact structure, low insertion loss, high-frequency selectivity, and the measured results agree with the simulated ones.

1. INTRODUCTION

The rapid development of wireless communication technology in recent years has dramatically stimulated the demand for multi-functional, multi-standard transceivers for frequency allocation and spatial coverage. In this trend, high-performance, easily integrated multi-passband filters are needed to support multiple non-contiguous channels simultaneously. Substrate integrated waveguide (SIW) multi passband filters with finite transmission zeros (TZs) have been widely investigated and applied to modern communication systems because of their high selectivity, small size, low cost, high power handling capability, and good planar integration [1].

In order to further improve the selectivity and out-of-band rejection levels of dual (multi)passband filters, scholars have conducted a lot of research and proposed several dual-passband SIW filter design methods based on them. The first approach uses two or more SIW cavities cascaded: Paper [2] proposes a quadrupole filter with SIW cavities cascaded. Although the proposed SIW filter can control the location of the transmission zeros well, the filter has poor stopband rejection due to strong bypass coupling. Papers [3–5] adopt a series cavity structure, and the input and output ports can be located on the same or different dielectric substrates. Filters with input and output ports on different dielectric substrates may have low integration with other planar circuits, and filters with input and output ports on the same dielectric substrate may have low stopband performance due to the influence of parasitic passband. The second method combines the SIW cavity with a planar slot line resonant structure. For example, coplanar waveguide (CPW) and complementary spilt ring resonator (CSRR) structures are used on the surface of the SIW cavity. In papers [6, 7], all the design parameters required for both passbands can be achieved through adding some additional resonators to the filter dual-mode resonant cavity to control the internal coupling and by determining the appropriate offset positions and coupling parameters to achieve the required cross-coupling coefficients for each of the two passbands. However, the special slot in the hybrid structure filter reduces the quality factor.

Received 28 July 2022, Accepted 9 September 2022, Scheduled 28 September 2022
* Corresponding author: Min Li (minminli2022@163.com).
The authors are with the School of Electronic and Information Engineering, Liaoning Technical University, Liaoning 125000, China.

In this paper, a novel dual-passband SIW filter structure is proposed, which is constructed by a loaded with a T-slot in a rectangular SIW cavity and two identical HMSIW cavities. The two HMSIW cavities are coupled with the magnetic field components of the SIW cavity, the TE_{101} mode in the two HMSIW cavities and the TE_{201} mode in the SIW cavity can provide a weak coupling path to produce two passbands. The T-slot can change the mode distribution in the cavity and reduce the center frequency of the first passband, while increasing the coupling path and producing an additional transmission zero. The hybrid coupling is achieved by adding two CPW resonators in the magnetic coupling window of the two cascaded resonant cavities. The added CPW resonators generate a new transmission zero, and the CPW resonators do not occupy additional SIW resonator circuit size. The proposed SIW filter structure has a flexible response with a transmission zero on each side of the passband to achieve steep out-of-band characteristics. The designed SIW filter has high selectivity, low loss performance, and compact size.

2. DESIGN OF DUAL-PASSBAND FILTER

2.1. Dual-Mode Characteristics of the SIW Cavity

The structure diagram of the rectangular SIW cavity is shown in Figure 1. W_{eff} and L_{eff} are the width and length of rectangular SIW cavity; D and S refer to the diameter of metal vias and the spacing between adjacent through holes. The rectangular SIW cavity can be equivalent to a rectangular waveguide cavity [8]. The derivation formulas of the resonant frequency and the frequency ratio of the basic mode to the higher-order mode are shown in (1)–(2):

$$f_{TEm0q} = \frac{c}{\sqrt{\mu_r \varepsilon_r}} \times \sqrt{\left(\frac{m}{W_{eff}}\right)^2 + \left(\frac{q}{L_{eff}}\right)^2} \tag{1}$$

$$\frac{f_{TEm0q}}{f_{TE101}} = \frac{\sqrt{\left(\frac{m}{W_{eff}}\right)^2 + \left(\frac{q}{L_{eff}}\right)^2}}{\sqrt{\left(\frac{1}{W_{eff}}\right)^2 + \left(\frac{1}{L_{eff}}\right)^2}} = \sqrt{q^2 + \frac{m^2 - q^2}{1 + \left(\frac{W_{eff}}{L_{eff}}\right)^2}} \tag{2}$$

where c is the propagation speed of electromagnetic waves in vacuum; ε_r and μ_r are the dielectric constant and permeability of the dielectric substrate; W_{eff} and L_{eff} are the equivalent width and length of the rectangular SIW cavity; m and q are the mode indicators along the x-axis and z-axis directions. From Equations (1) and (2), we know that when $m = q$:

$$\frac{f_{TE101}}{f_{TE101}} = 1; \quad \frac{f_{TE202}}{f_{TE101}} = 2; \quad \frac{f_{TE303}}{f_{TE101}} = 3 \tag{3}$$

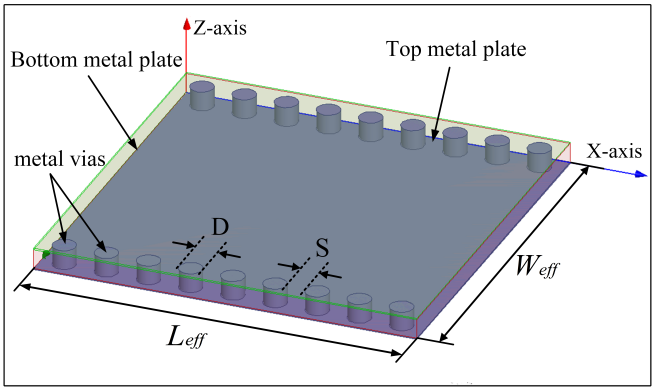

Figure 1. Rectangular SIW cavity structure.

When $\frac{W_{eff}}{L_{eff}} = k$, $m > q$:

$$\frac{f_{TE201}}{f_{TE101}} = \sqrt{1 + \frac{3}{1+k^2}}; \quad \frac{f_{TE301}}{f_{TE101}} = \sqrt{1 + \frac{8}{1+k^2}}; \quad \frac{f_{TE302}}{f_{TE101}} = \sqrt{4 + \frac{5}{1+k^2}}; \tag{4}$$

Similarly, when $m < q$:

$$\frac{f_{TE102}}{f_{TE101}} = \sqrt{4 - \frac{3}{1+k^2}}; \quad \frac{f_{TE103}}{f_{TE101}} = \sqrt{9 - \frac{8}{1+k^2}}; \quad \frac{f_{TE203}}{f_{TE101}} = \sqrt{9 - \frac{5}{1+k^2}}; \tag{5}$$

When $k = 1$, the mode resonances between TE_{201} and TE_{102}; TE_{301} and TE_{103}; TE_{302} and TE_{203} are equal for the dual-modes. Equations (2)–(5) calculate the normalized resonant frequencies of the six modes in the SIW cavity with different aspect ratios (W_{eff}/L_{eff}). The normalized frequencies of the six modes are shown in Figure 2.

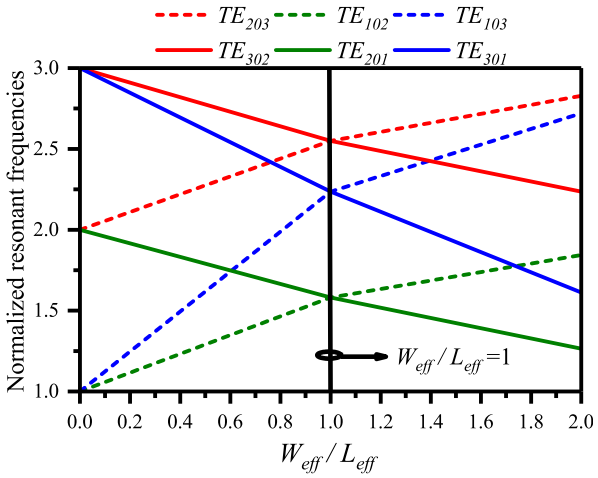

Figure 2. Normalized frequencies of the six modes.

In the rectangular SIW cavity used in this paper, when $W_{eff}/L_{eff} = 1$, TE_{201} and TE_{102} are a pair of two modes, and a transmission line is generated in the rectangular SIW cavity.

2.2. Dual-Passband with SIW Cavity Structure

Figure 3 shows the structure of the proposed filter. The left and right are two HMSIW cavities, and the middle is a rectangular SIW cavity. The two HMSIW cavities are coupled simultaneously with the SIW cavity through magnetic coupling windows, which are located on both sides of the dual-mode SIW cavity. The microstrip line is directly coupled with the HMSIW cavity, and the transition between the SIW cavity and microstrip line is realized by CPW, where L_3 and W_3 are the length and width of CPW.

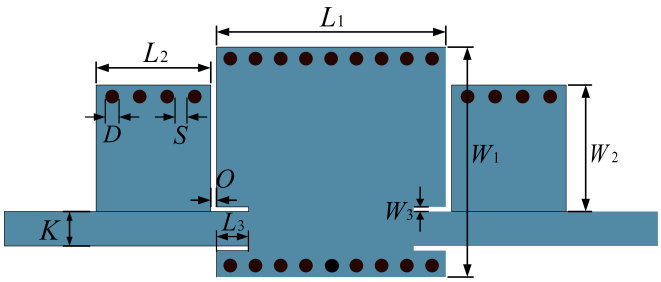

Figure 3. Dual-passband with SIW cavity structure.

To further illustrate the transmission principle of the proposed filter, the topology is shown in Figure 4. S and L represent the source and load of the filter, respectively. 1 and 4 are TE_{101} mode of HMSIW cavity, and 2 and 3 represent TE_{201} mode of the intermediate rectangular SIW.

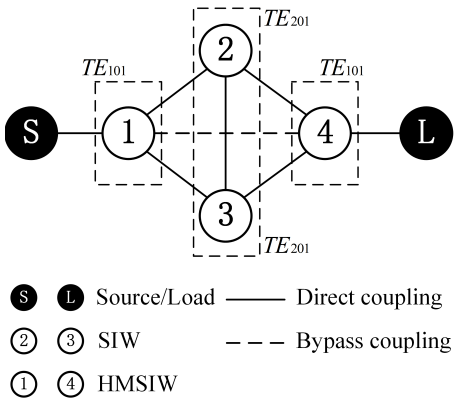

Figure 4. Dual-passband with SIW cavity topology.

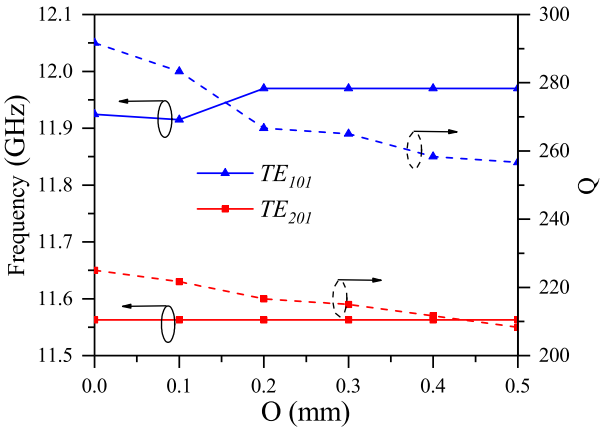

Figure 5. Relationship between resonant frequency, Q and O.

Since the input and output feeders are directly connected to the single-mode HMSIW resonant cavities, the electromagnetic field generated on the open side will provide the external coupling between adjacent resonant cavities, which is controlled by the size of O. Figure 5 shows the curves of resonant frequency and quality factor Q extracted from the model with offset O.

As shown in Figure 5, the resonant frequencies of the TE_{101} and TE_{201} modes do not change significantly as the offset O increases, but the quality factor Q decreases in both modes. In order to improve the quality factor, the offset O is finally determined to be 0.25 mm after optimization.

2.3. Transmission Response of a Dual-Pass Cavity with SIW

Figures 6(a) and (b) show the electric field distributions at 11.56 GHz and 11.96 GHz, for TE_{101} of HMSIW and TE_{201} of rectangular SIW. Two HMSIW cavities and one rectangular SIW cavity are coupled in series. The three resonant cavities operate simultaneously, with the first passband caused by the TE_{201} resonance of the SIW cavity and the second passband generated by the two HMSIW cavities TE_{101} resonantly generated to achieve a dual-passband. Due to the opposite coupling characteristics of TE_{201} and the two ports, this is a requirement for the emergence of the transmission zero TZ_1, as shown in Figure 7.

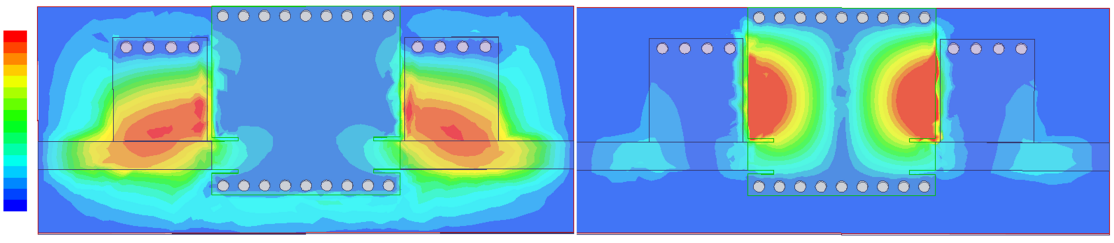

Figure 6. Electric field distribution in 11.56 GHz and 11.96 GHz cavities.

To further illustrate the transmission response of the proposed filter, Table 1 shows the modes and corresponding frequencies of the HMSIW cavity with three different lengths and widths. The

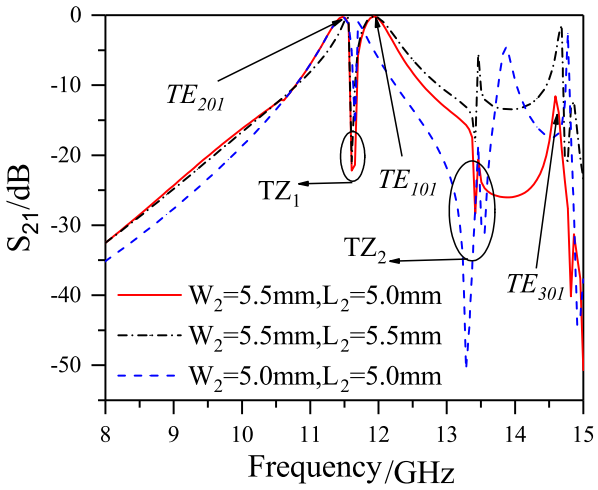

Figure 7. Transmission response in three different case.

Table 1. HMSIW parameters and simulation

Three different cases	HMSIW cavities Sizes (mm)	Mode	Frequency (GHz)	No. of parasitic passband
Case 1	$W_2 = 5 = 1/2W_1$ $L_2 = 5 = 1/2L_1$	TE_{101} TE_{201} TE_{203} TE_{301}	11.96 11.56 13.86 14.77	2
Case 2	$W_2 = 5.5 \neq 1/2W_1$ $L_2 = 5.5 \neq 1/2L_1$	TE_{101} TE_{201} TE_{203} TE_{301}	11.96 11.92 13.46 14.68	2
Case 3	$W_2 = 5.5 \neq 1/2W_1$ $L_2 = 5 = 1/2L_1$	TE_{101} TE_{201} TE_{301}	11.96 11.52 14.50	1

transmission response curve is shown in Figure 7. In the first case: the length and width of the two HMSIW cavities are the same, and they are half of the length and width of the rectangular SIW cavity, $W_2 = 5\,\text{mm} = 1/2W_1$, $L_2 = 5\,\text{mm} = 1/2L_1$. At this time, TE_{203} mode in HMSIW cavity and TE_{301} mode in rectangular SIW cavity generate two parasitic passbands at 13.86 and 14.77 GHz, respectively. In the second case: the length and width of the two HMSIW cavities are the same, but different from case 1, that is, $W_2 = 5.5\,\text{mm} \neq 1/2W_1$, $L_2 = 5.5\,\text{mm} \neq 1/2L_1$. TE_{203} mode in HMSIW cavity and TE_{301} mode in the rectangular SIW cavity generate two parasitic passbands at 13.46 and 14.68 GHz, respectively. In the third case: the length and width of the two HMSIW cavities are different, that is, $W_2 = 5.5\,\text{mm} \neq 1/2W_1$, $L_2 = 5\,\text{mm} = 1/2L_1$. The parasitic passband generated by TE_{203} mode in HMSIW cavity and TE_{301} mode in rectangular SIW cavity are attenuated. Considering the influence of parasitic passband generated by case 1 and case 2, the filter based on case 3 has better stopband performance.

Since the position of input feeder and output feeder is not on the center line of rectangular SIW cavity. In this case, the coupling between CPW structures is affected by the length and width of the CPW structure. The direction of the electric field is changed to form the second transmission zero TZ_2.

2.4. Design of Dual-Passband Filter with Loaded T-Slot

In this section, a T-slot structure is designed to change the field distribution inside a rectangular SIW cavity by a mode shift technique of slit perturbation, and the loaded T-slot structure double mode double passband SIW cavity structure diagram is shown in Figure 8. Etching this kind of slot structure on the dual-mode SIW cavity can shift the fundamental mode TE_{201} within the excitation cavity without changing its dimensions, which changes the first passband center frequency of the coupled SIW cavity from 11.52 GHz to 8.67 GHz with a 32.5% volume reduction. In addition, the path of the gap coupling in the dual-mode SIW cavity is increased after loading the T-slot, which can provide the out-of-band symmetric transmission zero TZ_3, and the resonant frequency of the dual-mode SIW cavity and the location of the transmission zero TZ_3 can be found by using the method of parity mode analysis [14, 15], as shown in Equations (6)–(8).

$$f_{even} \approx \frac{c}{4(C_L + C_W)\sqrt{\varepsilon_r}} \tag{6}$$

$$f_{odd} \approx \frac{c}{2(C_L + C_W + G_W)\sqrt{\varepsilon_r}} \tag{7}$$

$$f_{TZ_3} \approx \frac{c}{4(C_L + C_W + G_W)\sqrt{\varepsilon_r}} \tag{8}$$

From the above equation, it can be calculated that the center frequency of the first passband of the filter and the transmission zero TZ_3 are mainly influenced by the length of the T-slot and the length of the slit coupling slot. As shown in Figure 9, as the length of $C_L + C_W + G_W$ increases, the center

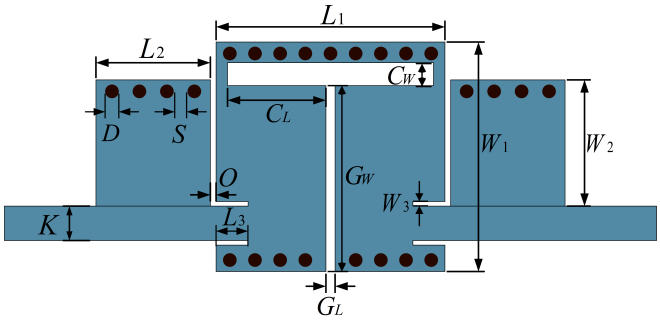

Figure 8. Loaded T-slot structure dual-passband with SIW cavity structure.

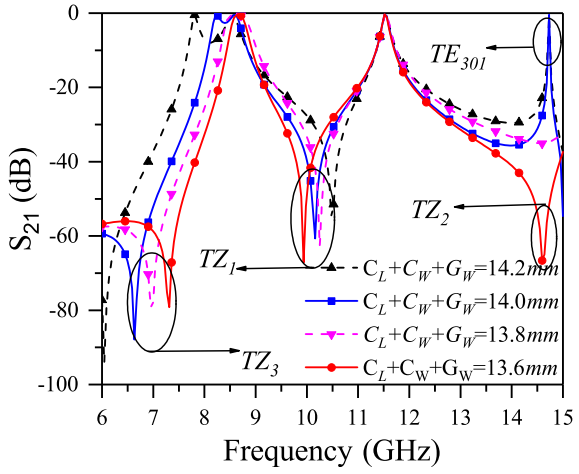

Figure 9. Effect of C_L, C_W, G_W on filter transmission characteristics.

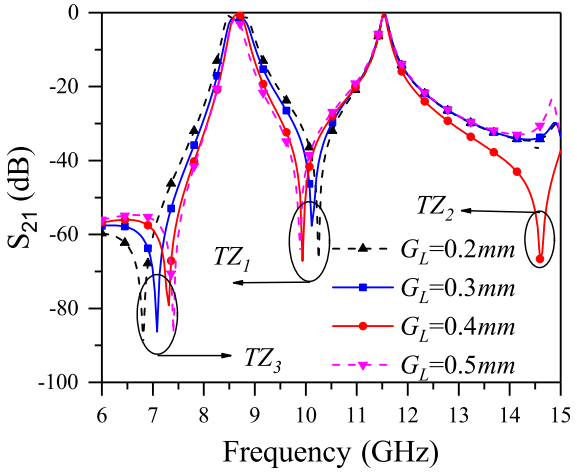

Figure 10. Effect of G_L on filter transmission characteristics.

frequency of the first passband of the filter and the transmission zero TZ_3 move to the lower frequency accordingly.

Since the vertical line slot is parallel to the field distribution line of TE_{201}, increasing the length of the vertical line of the T-slot thus increases the effect on the other higher modes except the fundamental mode, so the suppression of the parasitic passband TE_{301}. TE_{201} field distribution line is parallel to the T-slot, and the only effect of increasing the slot length on TE_{101} is to reduce the power capacity of the mode, which can lead to increased losses and reduced bandwidth.

Figure 10 shows the transmission curve of the loaded T-slot filter as a function of the gap width G_L. When it is 1 mm, it can be seen from Figure 10 that all resonances do not depend on G_L, and the center frequency of the first passband shifts slightly and then stabilizes as G_L becomes larger. The narrower the gap width of G_L is, the stronger the electric field and current density around the gap G_L are, resulting in increased conductive losses. The final gap width G_L was determined to be 0.4 mm.

3. MACHINING AND TEST RESULTS

The double passband filter proposed in this paper adopts a Rogers rt/duriod 5880 substrate with thickness of 0.508 mm and dielectric constant of 2.2. Three-dimensional electromagnetic simulation software HFSS 15.0 is used for simulation and optimization. The optimized parameters are shown in Table 2. The results of simulation and measurement are shown in Figure 11 and Figure 12. The measured center frequencies are 8.67 GHz and 11.52 GHz, respectively, and the corresponding relative bandwidths are 3.13% and 1.18%. The maximum insertion loss in the band is 0.48 dB and 0.31 dB, and the return loss is 26.31 dB and 22.56 dB. The isolation between the two passbands is up to 67.15 dB, and three transmission zeros are generated outside the passbands. Two transmission zeros are generated

Table 2. Filter sizes parameters.

Parameters	Value (mm)	Parameters	Value (mm)	Parameters	Value (mm)
L_1	10.00	W_1	10.00	C_W	1.00
L_2	5.00	W_2	5.50	C_L	4.30
L_3	0.20	W_3	1.40	G_W	8.10
D	0.30	O	0.25	G_L	0.40
S	0.80	K	1.50		

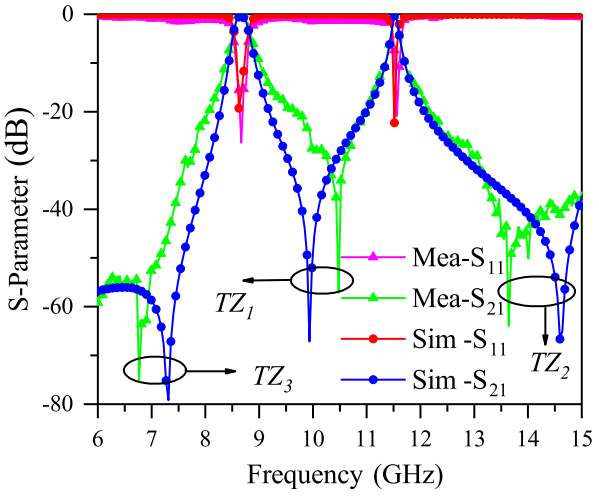

Figure 11. The simulated and measured results of Filter.

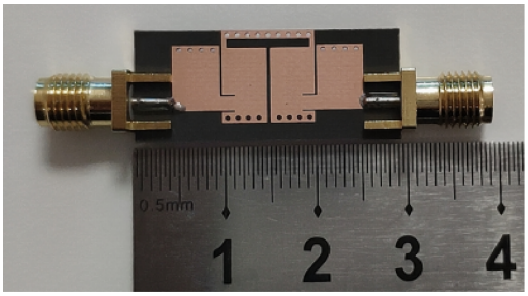

Figure 12. A real diagram of a dual-passband filter.

between the two passbands, which greatly improves the isolation performance of the two passbands. The transmission zero above the second passband increases the roll rate of the bandpass filter attenuation. The suppression between 6.80 GHz and 10.67 GHz in the high-frequency band is greater than 38 dB.

As can be seen from Figure 11, the measured filter in-band insertion loss, return loss, and isolation between the two passbands are somewhat different compared with the simulation results, and there are three main reasons for this difference. Firstly, the radiation occurs in the plane parallel to the ground inside the waveguide, and it is limited by the through-wall; secondly, the structure used in this paper is not a completely closed structure, and it has slot coupling, so the filter exhibits a larger radiation loss; finally, due to the processing error of the device, the loss of the metal and the loss of the SMA connector will also have some influence on the measured results [16, 17]. The test results are consistent with the simulation, which shows that the proposed filter can achieve high selectivity with dual-passbands.

In order to highlight the characteristics of the filter such as small size, high selectivity, and low loss, the filter designed in this paper is compared with some similar state-of-the-art designs in Table 3. The comparison shows that the filters in this paper have significant advantages in terms of structure size and transmission characteristics. In general, the filter designed in this paper has low insertion loss, more compact size, and good out-of-band rejection with good overall performance compared to some existing literature. The proposed filter has the following advantages: 1) more compact structure and easier design because the large and complex elliptical structure of SIW is not used; 2) better isolation between the two channels due to steeper rejection (67.2); 3) wider rejection band and higher attenuation due to the absence of resonance in the T-slot (79.2 dB at 7.3 GHz, 66.6 dB at 14.6 GHz).

Table 3. Comparison of the parameters of this filter and other filters.

Ref.	Center frequency (GHz)	IL (dB)	RL (dB)	FBW (%)	No. of TZ_s	Size λ_g^2
[1]	24.97\26.70	2.00\2.50	20.0\40.0	5.41\5.25	2	1.50×2.67
[2]	15.97\18.31	1.14\0.76	20.0\30.0	1.70\2.50	3	1.86×2.02
[5]	8.000\10.00	2.25\1.92	51.0\46.0	3.50\6.00	1	$\pi \times 0.65$
[6]	5.300\8.500	2.02\1.82	15.0\21.0	6.26\7.75	4	0.84×1.31
[7]	33.55\38.00	5.00\2.20	12.0\10.0	2.68\3.68	1	0.63×1.50
[9]	6.220\8.240	0.86\1.32	41.0\36.0	7.70\3.90	3	0.41×0.89
[10]	26.73\31.52	0.48\0.67	12.0\20.0	3.60\2.00	3	1.34×2.55
[11]	12.00\17.00	1.16\2.32	21.0\12.0	6.87\3.26	5	0.95×1.22
[12]	2.400\5.200	1.40\1.60	20.2\12.0	7.50\5.77	0	0.07×0.17
[13]	2.700\3.200	1.14\1.32	24.0\66.0	7.78\6.25	3	0.44×0.44
This work	8.671\11.52	0.48\0.31	26.3\22.6	3.13\1.18	3	0.34×0.81

4. CONCLUSION

In this paper, the dual-mode resonant characteristics of SIW are systematically analyzed and described. Based on this characteristic, a new dual-passband, wide-stopband filter design method is given. The filter is formed by the TE_{201} mode in the SIW cavity and two identical TE_{101} mode-based HMSIW resonant cavities to form the dual-passband, focusing on the suppression of parasitic passband by the coupling window between the SIW cavity and the HMSIW cavity, the loading of T-slot to add additional transmission zero, and a detailed study of the relationship between the coupling mode and the frequency response. The simulated results of the designed SIW dual-passband, wide-stopband filter agree well with the measured ones making it well suited for radar or satellite communication applications.

ACKNOWLEDGMENT

This work was supported by the National Natural Science Foundation of China (No: 61971210).

REFERENCES

1. Chu, P., W. Hong, M. Tuo, K.-L. Zheng, W.-W. Yang, F. Xu, and K. Wu, "Dual-mode substrate integrated waveguide filter with flexible response," *IEEE Transactions on Microwave Theory and Techniques*, Vol. 65, No. 3, 824–830, 2017.
2. Wang, S., D. Zhang, J. Liang, Q.-Q. Yuan, L. Liu, and L.-Q. Wu, "SIW dual-mode dual-band balanced filter with closely spaced passbands," *2020 Cross Strait Radio Science & Wireless Technology Conference (CSRSWTC)*, 1–2, Fuzhou, China, 2020.
3. Zhou, K., C.-X. Zhou, H.-W. Xie, and W. Wu, "Synthesis design of SIW multiband bandpass filters based on dual-mode resonances and split-type dual-and triple-band responses," *IEEE Transactions on Microwave Theory and Techniques*, Vol. 67, No. 1, 151–161, 2019.
4. Hizamel, M., C. Ian, and I. Alaa, "Integrated dual-band radiating bandpass filter using dual-mode circular cavities," *IEEE Microwave and Wireless Components Letters*, Vol. 21, No. 5, 246–248, 2011.
5. Han, Y.-K., H.-W. Deng, J.-M. Zhu, S.-B. Xing, and W. Han, "Compact dual-band dual-mode SIW balanced BPF with intrinsic common-mode suppression," *IEEE Microwave and Wireless Components Letters*, Vol. 31, No. 2, 101–104, 2021.
6. Zhou, K., C.-X. Zhou, and W. Wu, "Dual-mode characteristics of half-mode siw rectangular cavity and applications to dual-band filters with widely separated passbands," *IEEE Transactions on Microwave Theory and Techniques*, Vol. 66, No. 11, 4820–4829, 2018.
7. He, Z.-S., Z.-H. Shao, X. Li, and M.-K. Shen, "A dual-band bandpass filter based on hybrid structure of substrate integrated waveguide and substrate integrated coaxial line," *2016 IEEE MTT-S International Microwave Symposium (IMS)*, 1–4, San Francisco, CA, USA, 2016.
8. Zhang, H., W. Kang, and W. Wu, "Miniaturized dual-band differential filter based on CSRR-loaded dual-mode SIW cavity," *IEEE Microwave and Wireless Components Letters*, Vol. 28, No. 10, 897–899, 2018.
9. Dong, H.-K., J.-Y. Mo, Y.-H. He, Z.-W. Ma, and X.-X. Yang, "Design of a millimeter-wave dual-band bandpass filter using SIW dual-mode cavities," *2016 IEEE MTT-S International Wireless Symposium (IWS)*, 1–3, Shanghai, China, 2016.
10. Zhou, K., C.-X. Zhou, and W. Wu, "Substrate-integrated waveguide dual-mode dual-band bandpass filters with widely controllable bandwidth ratios," *IEEE Transactions on Microwave Theory and Techniques*, Vol. 65, No. 10, 3801–3812, 2017.
11. Shen, W., W.-Y. Yin, and X.-W. Sun, "Miniaturized dual-band substrate integrated waveguide filter with controllable bandwidths," *IEEE Microwave and Wireless Components Letters*, Vol. 21, No. 8, 418–420, 2011.

12. Li, P., H. Chu, and R.-S. Chen, "Design of compact bandpass filters using quarter-mode and eighth-mode SIW cavities," *IEEE Transactions on Components, Packaging and Manufacturing Technology*, Vol. 7, No. 6, 956–963, 2017.
13. Liu, Q., D.-F. Zhou, S.-X. Wang, and Y. Zhang, "Highly-selective pseudoelliptic filters based on dual-mode substrate integrated waveguide resonators," *Electronics Letters*, Vol. 52, No. 14, 1233–1235, 2016.
14. Liu, Q., D.-W. Zhang, M. Tang, H.-L. Deng, and D.-F. Zhou, "A class of box-like bandpass filters with wide stopband based on new dual-mode rectangular SIW cavities," *IEEE Transactions on Microwave Theory and Techniques*, Vol. 69, No. 1, 101–110, 2020.
15. Liu, Q., D.-F. Zhou, Y. Zhang, D.-W. Zhang, and D.-L. Lv, "Substrate integrated waveguide bandpass filters in box-like topology with bypass and direct couplings in diagonal cross-coupling path," *IEEE Transactions on Microwave Theory and Techniques*, Vol. 67, No. 3, 1014–1022, 2019.
16. Zhou, K., C.-X. Zhou, and W. Wu, "Substrate integrated waveguide dual-mode dual-band filter with multilayered configuration," *2017 IEEE Electrical Design of Advanced Packaging and Systems Symposium (EDAPS)*, 1–3, Haining, China, 2019.
17. Sun, J.-H., D.-W. Zhang, Q. Liu, and X. Wang, "Dual-mode dual-band substrate integrated waveguide bandpass filter with improving the spurious passband," *2018 International Conference on Microwave and Millimeter Wave Technology (ICMMT)*, 1–3, Chengdu, China, 2018.